

# Curve crossing and negative refraction in simulations of near-field coupled metallic nanoparticle arrays

Kenneth Lopata<sup>a)</sup> and Daniel Neuhauser  
*Chemistry and Biochemistry Department, University of California,  
 Los Angeles, California 90095-1569, USA*

Roi Baer  
*The Fritz Haber Center for Molecular Dynamics and the Department of Physical Chemistry,  
 The Hebrew University, Jerusalem 91904, Israel*

(Received 15 May 2007; accepted 13 September 2007; published online 18 October 2007)

We extend our previous results [R. Baer *et al.*, *J. Chem. Phys.* **126**, 014705 (2007).] to develop a simple theory of localized surface plasmon-polariton (LSPP) dispersion on regular arrays of metal nanoparticles in the weak-field and weak-damping limits. This theory describes the energy-momentum as well as the polarization-momentum properties of LSPP waves, both of which are crucial to plasmonic device design. We then explicitly compute the dispersion relation for isotropic and anisotropic two-dimensional square lattices, and show curve crossings between all three levels as well as negative refraction where the phase and group velocities (refractive indices), or at least their projection along the main axis, have different signs. The curve crossing implies that scattering between the different polarizations, and therefore different velocities, is easy at the curve crossing momenta, so that a quick change in wave packet direction can be achieved. Time-resolved wave packet dynamics simulations demonstrate negative refraction and the easy scattering over nanometer length scales. This paper also gives some computational schemes for future applications, such as a way to include source terms and how to efficiently treat dissipative effects. © 2007 American Institute of Physics. [DOI: [10.1063/1.2796162](https://doi.org/10.1063/1.2796162)]

## I. INTRODUCTION

Recent theoretical<sup>2-4</sup> and experimental<sup>5,6</sup> studies have demonstrated the feasibility of using metal nanoparticle arrays to guide electromagnetic energy of optical frequencies along geometries smaller than the diffraction limit of light. This transfer of energy is accomplished via near-field coupling between localized surface plasmons on each nanoparticle, resulting in a localized surface plasmon polariton (LSPP) wave propagating along the device. Additionally, metamaterials have been constructed which exploit surface plasmons to exhibit negative refractive index<sup>7</sup> at microwave frequencies. Such devices may one day be used to build “superlenses” capable of using visible light to resolve features much smaller than optical wavelengths.<sup>8,9</sup> An understanding of the novel dispersive properties of LSPP waves and the ability to perform large-scale simulations of potential plasmonic devices are crucial to the further development of this field.

Various approaches are taken to model plasmonic devices, including computationally expensive complete solutions of Maxwell’s equations using finite difference time domain schemes,<sup>2,10</sup> point-dipole and coupled nanoparticle approximations,<sup>3,11</sup> time-dependent density functional theory,<sup>12</sup> and plasmon hybridization schemes.<sup>13</sup> In a recent paper,<sup>1</sup> we introduced a quantum mechanical approach based on the exciton mode formalism, which we used to explore

both the dispersion properties of one-dimensional arrays of nanoparticles as well as LSPP dynamics on both one- and two-dimensional lattices.

In this paper, we extend our previous results<sup>1</sup> to develop a dispersion relation for a two-dimensional lattice of metal nanoparticles in the weak-damping and weak-field limits, and also compare these results with time-resolved wave packet calculations that demonstrate the ability of this type of system to exhibit negative refractive index.

The calculations are vastly simplified by taking the weak-damping limit, but in reality surface plasmon excitations on any nanoparticle are highly damped. This damping comes from radiative losses, plasmon-phonon coupling in the nanoparticle, and coupling to electronic levels in the surrounding substrate/matrix material.<sup>14</sup> For any currently realizable system, this damping makes coherent LSPP transfer impossible for chains longer than a few nanoparticles. Although the weak-damping approximation is quite drastic, the resulting formalism is still adequate enough to qualitatively describe the dispersion (energy and momentum) and dynamical properties of LSPP-based devices. More importantly, the formalism gives a transparent, illustrative, and intuitive picture.

## II. THEORY

Here, we outline a simple yet effective method to analytically compute the dispersion relation of a one-, two-, or three-dimensional array of nanoparticles. Although the computational part of this study was limited to a simple square

<sup>a)</sup>Electronic mail: [lopata@chem.ucla.edu](mailto:lopata@chem.ucla.edu)

two-dimensional lattice, the method is also applicable to three-dimensional crystals. As before,<sup>1</sup> we make the low-damping and weak-field approximations, and assume spherical symmetry on each nanoparticle such that each particle can support three orthogonal surface plasmon modes, corresponding to  $x$ ,  $y$ , and  $z$  oriented electron oscillations, respectively. Thus, to describe a lattice of  $N$  particles, we require a Hilbert space spanned by  $3N$  functions  $\Psi_{n,\alpha}$ , where  $n = 1, 2, \dots, N$  is the nanoparticle index and  $\alpha = 1, 2, 3$  represents the three orthogonal polarizations  $x, y, z$ .

The ‘‘Hamiltonian’’ associated with the interaction of the polarization can be written as

$$H = H_0 + H_c, \quad (1)$$

where  $H_0$  is a diagonal matrix with elements that are the excitation frequency  $\omega_n$  of each dipole, while  $H_c$  is an off-diagonal coupling Hamiltonian, which can be written in the following schematic form:

$$H_c(\mathbf{x}_n, \mathbf{x}_m) = \xi^2 \nabla \nabla \frac{1}{|\mathbf{x}_n - \mathbf{x}_m|}, \quad (2)$$

where  $\xi$  is the transition dipole moment of the nanoparticles and  $|\mathbf{x}_n - \mathbf{x}_m|$  is the separation between particles  $n$  and  $m$ . We use atomic units, where  $\hbar = m_e = 1$ ; note that in these units  $e^2/4\pi\epsilon_0 = 1$ , and the velocity of light is  $c = 137.036$  a.u.

In an explicit form, the matrix elements of  $H$  for the interaction of polarization  $\alpha$  on site  $n$  with polarization  $\beta$  on site  $m$  is

$$H_{n\alpha, m\beta} = \begin{cases} \omega_n \delta_{\alpha\beta}, & n = m \\ -\frac{\xi^2}{|R_{nm}|^5} [\delta_{\alpha\beta} |R_{nm}|^2 - 3(R_{nm})_\alpha (R_{nm})_\beta], & n \neq m, \end{cases} \quad (3)$$

where  $R_{nm} = |\mathbf{x}_n - \mathbf{x}_m|$ . This Hamiltonian governs the motion of time-dependent excitations, through

$$i \frac{d\Psi}{dt} = H\Psi, \quad (4)$$

where we introduced the wave function associated with the excitations. In the ‘‘Relation to Electrodynamics’’ section below, we discuss in greater depth the connection between this ‘‘quantum-mechanical’’ model and electrodynamics and show that the wave function amplitude  $\Psi_{n\alpha}$  is the polarization in the media in direction  $\alpha$ . We also show how it is possible to include an external exciting field in the equation and how, in principle, to treat dissipative effects by changing the transition dipole moment into a time-dependent memory term for previous times.

For a homogenous system, the eigenfunctions of  $H$  can be written in a separable form, as

$$\Psi_{n\alpha} = \psi_n \eta_\alpha. \quad (5)$$

The dispersion relation  $\omega_p(\mathbf{k})$  can be calculated from the Schrödinger equation according to

$$H\Psi = \omega_p(\mathbf{k})\Psi, \quad (6)$$

$$\sum_{m=1}^N \sum_{\beta=1}^3 H_{n\alpha, m\beta} \psi_m \eta_\beta = \omega_p(\mathbf{k}) \psi_n \eta_\alpha, \quad (7)$$

where  $n = 1, 2, \dots, N$  is an index over the nanoparticles and  $p = 1, 2, 3$  is an index over the polarization vector (i.e., designates the  $p$ th eigenvector  $\eta_{jp}$  and we often omit the  $p$  index). The summations over  $m$  and  $\beta$  are likewise over particle number and polarization, respectively. In the large  $N$  limit or for periodic systems, we know that the spatial part of the wave function  $\psi_n$  is simply a plane wave of the form  $\psi_n = e^{i\mathbf{k}\cdot\mathbf{r}_n}$ . Additionally, since all sites on the lattice are the same, we can choose to look at the wave function on the first site ( $n=1$ ) with  $\mathbf{r}_1 = (0, 0, 0)$ , which simplifies Eq. (7) to

$$\sum_{m=1}^N \sum_{\beta=1}^3 H_{1\alpha, m\beta} e^{i\mathbf{k}\cdot\mathbf{r}_m} \eta_{\beta p} = \omega_p(\mathbf{k}) \eta_{\alpha p}. \quad (8)$$

Now, we convert the sum over particle index  $m$  in Eq. (8) into a triple sum over discrete positions, with grid spacings of  $a_x, a_y$ , and  $a_z$ , respectively,

$$\sum_{n_x, n_y, n_z} \sum_{\beta=1}^3 H_{0\alpha, r\beta} e^{i\mathbf{k}\cdot\mathbf{r}} \eta_{\beta p} = \omega_p(\mathbf{k}) \eta_{\alpha p}, \quad (9)$$

where  $\mathbf{r} = (n_x a_x, n_y a_y, n_z a_z)$ . The triple sum in Eq. (9) can then be readily computed using a three-dimensional fast Fourier transform

$$\sum_{n_x, n_y, n_z} H_{0\alpha, r\beta} e^{i\mathbf{k}\cdot\mathbf{r}} \equiv F_{\alpha\beta}(\mathbf{k}), \quad (10)$$

giving

$$\sum_{\beta=1}^3 F_{\alpha\beta}(\mathbf{k}) \eta_{\beta p} = \omega_p(\mathbf{k}) \eta_{\alpha p}. \quad (11)$$

All that remains, then, is to solve for the three eigenvalues and eigenvectors of Eq. (11) for each value of  $k_x, k_y$ , and  $k_z$ .

The three resultant eigenvalue surfaces,  $\omega_1(\mathbf{k})$ ,  $\omega_2(\mathbf{k})$ , and  $\omega_3(\mathbf{k})$ , are the adiabatic energy surfaces of the first, second, and third lowest energy eigenstates, while the three eigenvectors at each  $\mathbf{k}$  represent the relative mixture of  $x$ ,  $y$ , and  $z$  polarizations of these eigenstates. This mixture of polarizations is a direct consequence of the coupling between the three orthogonal ( $x, y, z$ ) local surface plasmon modes between individual nanoparticles in the Hamiltonian (3). In three dimensions, therefore, where all three are coupled, the eigenstates are generally not pure but rather a mixture of  $x$ ,  $y$ , and  $z$  polarizations. In two dimensions where  $z$  is decoupled from  $x$  and  $y$ , one of the eigenstates is pure  $z$  and the other two are mixed  $xy$ , and in one dimension all surface plasmon modes are decoupled, so all eigenstates are pure.

### III. RESULTS

#### A. Dispersion relation

Here, we describe the results of the theory as applied to a two-dimensional regular square lattice of nanoparticles. The simulations scale with the size of the dots (as long as the

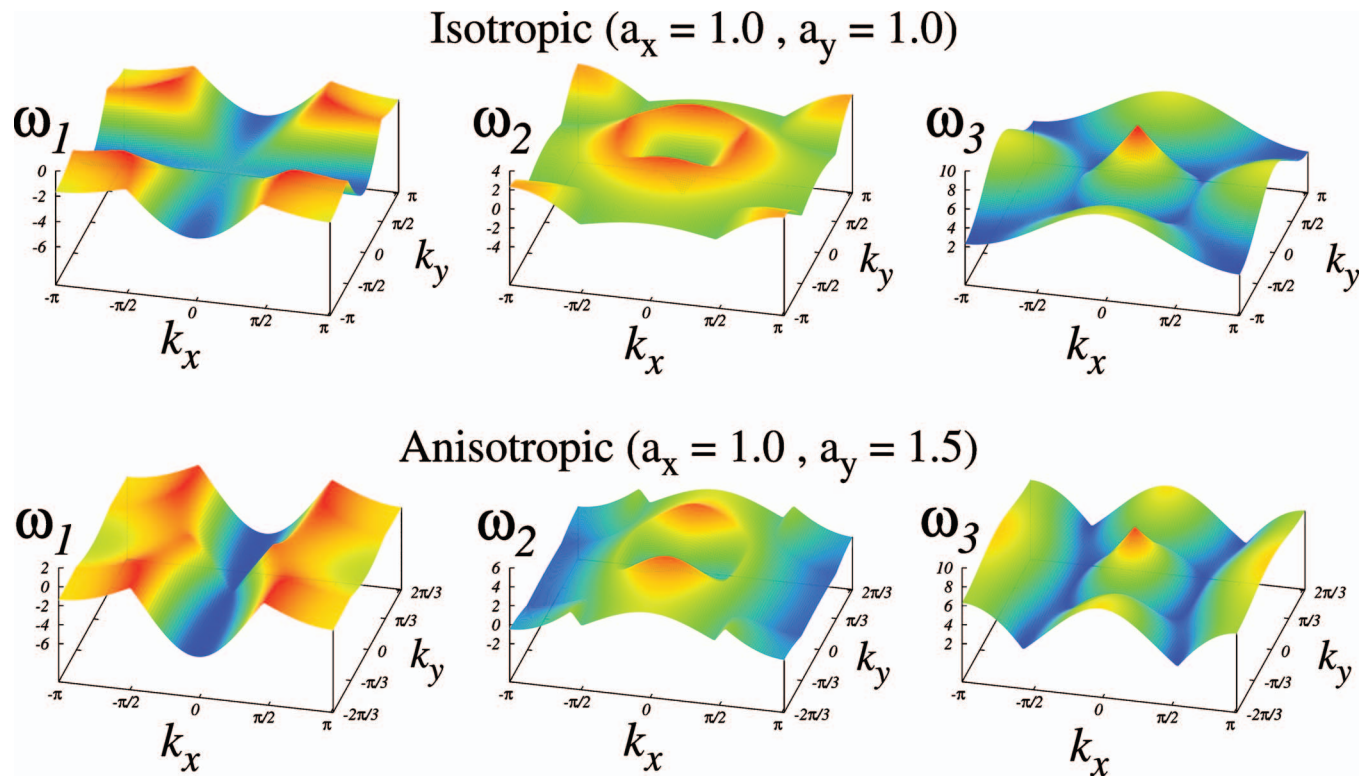


FIG. 1. (Color) The three adiabatic energy (eigenvalue) surfaces for the isotropic lattice (top) and the anisotropic lattice (bottom). The sharp features around  $\mathbf{k}=\mathbf{0}$  in the  $\omega_2$  and  $\omega_3$  surfaces are artificial and due to the singularity at that point. See the discussion for the meaning of the energy units.

ratio of nanoparticle size to spacing is held fixed). We have therefore used scaled atomic units. The simulations were done where the spacing of the nanoparticles in the  $x$  axis is the basic length unit, and the energy is measured in units of  $\xi^2/a^3$ , where  $a$  is the lattice spacing. Typical coupling strengths have been measured and calculated to be a few tenths of an eV.<sup>5</sup>

We now present the dispersion relations for two particular examples: An isotropic lattice with spacings  $a_x=a_y=1.0$  and an anisotropic lattice with  $a_x=1.0$  and  $a_y=1.5$ . Our subsequent analysis will focus on the anisotropic lattice, which displays interesting phenomena not seen in the isotropic one, such as broad curve crossing and negative refractive index. We include, however, the results for the isotropic lattice for comparison.

Figure 1 shows the three eigenvalue surfaces of Eq. (11) for both an isotropic lattice with spacings  $a_x=a_y=1.0$  (top) and an anisotropic lattice with  $a_x=1.0$  and  $a_y=1.5$  (bottom). In both cases, the lattices were  $128 \times 128$  nanoparticles large to facilitate taking the fast Fourier transform (FFT). The anisotropy of the lattice introduces a clear asymmetry into the adiabatic surfaces and also contracts the first Brillouin zone in the  $k_y$  direction.

As the energy units are scaled, this figure (i.e., Fig. 1) applies generally for a dipolar system of any size or material. For concreteness, the longitudinal coupling energy for metal particles is two times the basic unit, which is  $\xi^2/a^3$ . Furthermore, for metal particles, we can write,  $\xi=\kappa b^{3/2}$ , where  $b$  is the radius of the particles. Our energies, therefore, are calculated in terms of the basic parameter  $\kappa^2(b/a)^3$ . For the specific example of gold particles with an interparticle spacing

of three times their radius,  $\kappa^2 \sim 1.3$  eV, so we conclude that our basic energy unit is approximately 1.3 eV. Thus, the basic energy unit (i.e., “1” on the plots) would be 0.05 eV. Further, note that our zero energy is the frequency of the light, which is a constant that we subtract from the energy. As such, negative energies are frequencies lower than that of the light and positive energies are higher frequencies.

Of particular interest is the intersection of these three adiabatic surfaces, which corresponds to particular momenta where there is a ready conversion between different LSPP eigenmodes. Figure 2 shows the differences between the second and first surfaces and the third and second ones, respectively, for both the isotropic and anisotropic lattice. The ring shaped region of intersection of  $\omega_1$  and  $\omega_2$  is significantly broadened in the anisotropic lattice, which is visible as two bands around  $k_y = -(\pi/3)$  and  $\pi/3$ . This broad range of intersection can be seen clearly when slices of the three  $\omega(\mathbf{k})$  surfaces are viewed for fixed values of  $k_y$ , as in Fig. 3 (for the meaning of the energy units, see the discussion of Fig. 1).

To completely describe the eigenstates, we also need to consider the eigenvectors. The three eigenvectors of Eq. (11) at each value of  $\mathbf{k}$  describe the relative proportion of  $x$ ,  $y$ , and  $z$  polarizations of the three eigenmodes. On this two-dimensional lattice, one of the eigenmodes must correspond to pure  $z$  polarization, while the other two are generally mixed  $xy$ . Figure 4 shows, for the anisotropic lattice, the azimuthal ( $\phi$ ) and zenith ( $\theta$ ) angles of the first (lowest energy) eigenvector as a function of  $k_x$  for four values of  $k_y$ .

The jumps in eigenvector angle, which correspond to switching of the lowest energy eigenstate among the three possible modes (two  $xy$ ; one  $z$ ), occur at the curve crossing

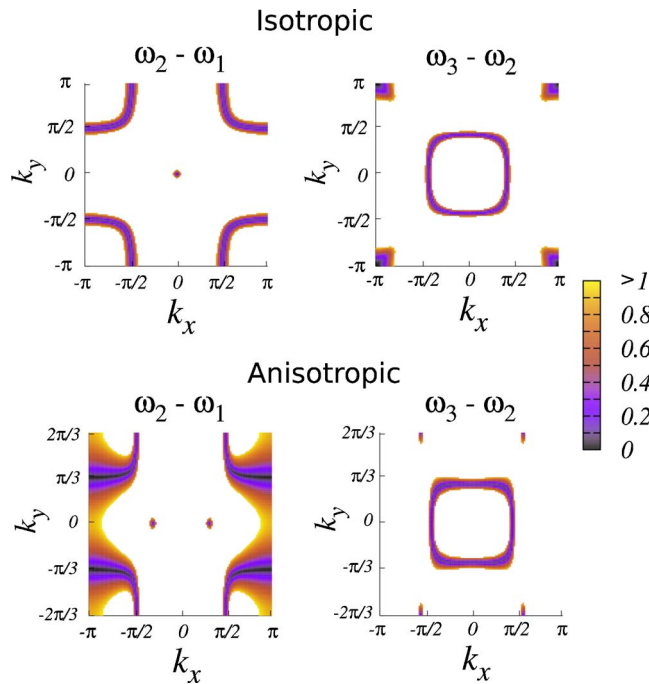


FIG. 2. (Color online) Contour plots of  $\omega_2(\mathbf{k}) - \omega_1(\mathbf{k})$  and  $\omega_3(\mathbf{k}) - \omega_2(\mathbf{k})$ , illustrating regions of intersection between the three adiabatic surfaces. The intersection is significantly more pronounced in the anisotropic lattice (bottom) than in the isotropic one (top).

momenta between the  $\omega_1$  and  $\omega_2$  adiabatic energy surfaces (see the dark bands in Fig. 2 and intersections in Fig. 3). For example, when  $k_y=0$ , the lowest eigenmode switches from being pure  $x$  to pure  $y$  at  $k_x \cong \pi/4$ .

Of particular note is that the lowest energy eigenmode is mostly pure  $x$  ( $\phi=0^\circ$ ,  $\theta=90^\circ$ ) for a range of  $k_x$  values around 0, and this range is large only for momenta away from the intersection bands. When the angles of the other two eigen-

vectors are also considered (not shown), for each given momentum one of the three eigenmodes of this two-dimensional lattice is indeed pure  $z$  ( $\theta=0^\circ$ ), while the other two are, in general, an  $xy$  mixture, as predicted from the Hamiltonian (3).

Also of interest are the group and phase velocities of the LSPP waves, which are defined as

$$v_p^\alpha = \frac{\omega(\mathbf{k}) - \omega(\mathbf{0})}{k_\alpha} \quad (12)$$

and

$$v_g^\alpha = \frac{\partial \omega(\mathbf{k})}{\partial k_\alpha}, \quad (13)$$

respectively (with  $\alpha=x,y,z$ ). The second term in Eq. (12) corresponds to choosing the zero energy to be at  $\mathbf{k}=\mathbf{0}$ . The derivative in Eq. (13) is conveniently calculated in reciprocal space using a FFT according to

$$\frac{\partial \omega(\mathbf{k})}{\partial k_\alpha} = \text{FFT}\{ir_\alpha \tilde{\omega}(\mathbf{r})\}, \quad (14)$$

where  $\tilde{\omega}(\mathbf{r})$  is the inverse fast Fourier transform of  $\omega(\mathbf{k})$ .

Figure 5 shows the  $y$  phase and group velocities for the lowest energy eigenmode of the anisotropic lattice for fixed  $k_x=\pi/2$ . Although the singularity around  $k_y=0$  overwhelms the shape of the phase velocity curve, it is clear that for a large region between  $k_y \cong \pi/2$  and  $3\pi/2$ , the phase velocity has the opposite sign of the group velocity. This is a feature of negative refractive index, and its implications are further explored in the following section.

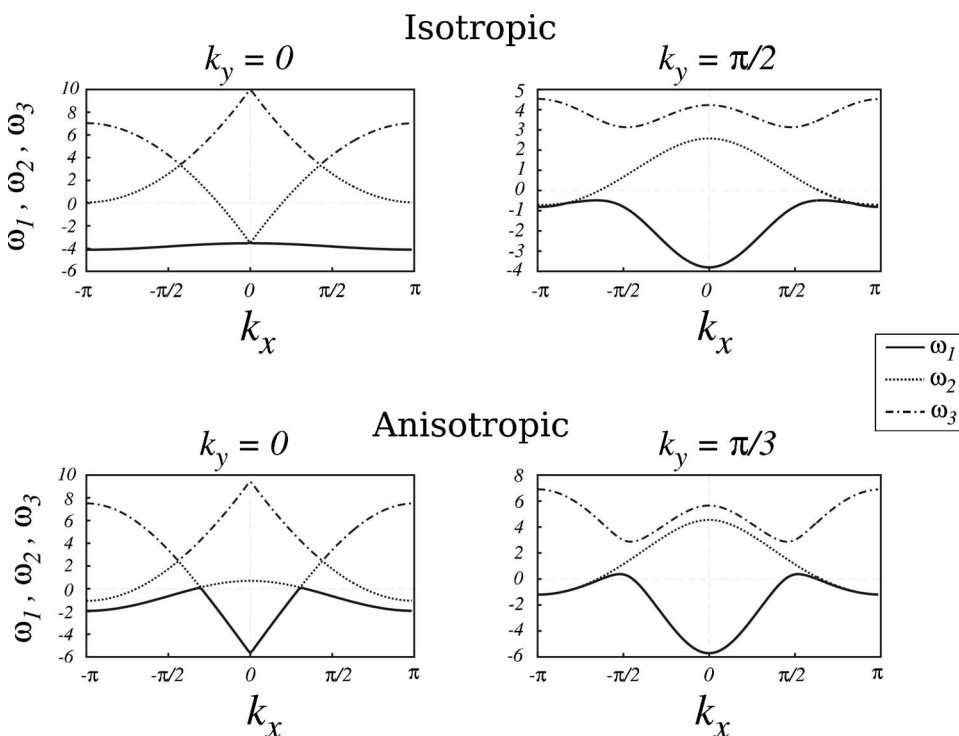


FIG. 3. Slices of the first (solid), second (dashed), and third (dash-dotted) dispersion surfaces for the isotropic lattice (top) and the anisotropic lattice (bottom). The two figures on the left correspond to  $k_y=0$ , while the two at the right occur at one of the broad bands of intersection ( $k_y=\pi/2$  for the isotropic lattice;  $k_y=\pi/3$  for the anisotropic lattice).

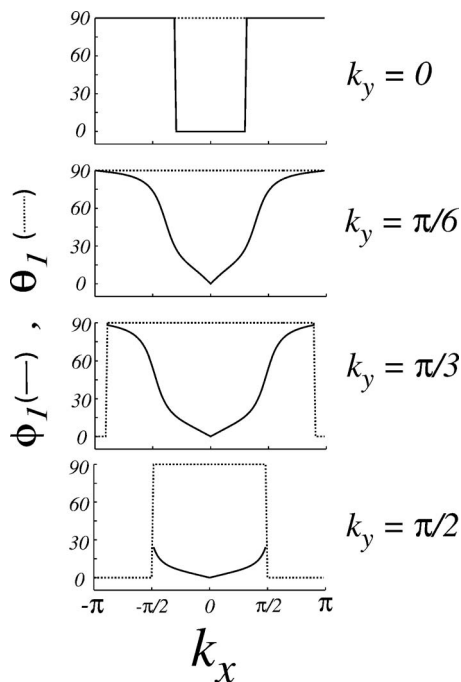


FIG. 4. The azimuthal ( $\phi$ , solid) and zenith ( $\theta$ , dashed) angles of the first eigenvector of the anisotropic lattice for various values of  $k_y$ . The direction of the eigenvectors corresponds to the relative proportion of  $x$ ,  $y$ , and  $z$  surface plasmon polarizations of the eigenstate. The jumps in angle occur at the  $\omega_1$  and  $\omega_2$  curve crossing momenta and correspond to switches among the three possible eigenpolarizations (two  $xy$  and one  $z$ ). When the state is pure  $z$  ( $\theta=90^\circ$ ), the azimuthal angle is not well defined and is thus omitted.

## B. Dynamical simulation

Here, we compare the results of the dispersion relation to a LSPP dynamics simulation of a simple hypothetical device consisting of a two-dimensional lattice of 2100 ideal metal nanoparticles patterned on a flat substrate, whose effects we ignored. We take the interparticle spacing to be the same as the above studied anisotropic square lattice ( $a_x=1.0$ ;  $a_y=1.5$ ), and additionally introduce a step perturbation by shifting the  $y$  location of the nanoparticles on the right half of the slab by  $\Delta y$ .

An initial pure  $x$  polarization Gaussian wave packet of the form

$$\psi_x(\mathbf{r};0) = \exp\left(-\frac{|\mathbf{r}-\mathbf{r}_0|^2}{2\sigma^2} + \mathbf{k} \cdot (\mathbf{r}-\mathbf{r}_0)\right), \quad (15)$$

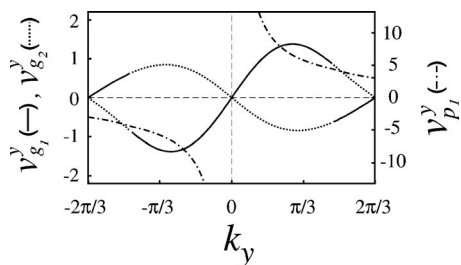


FIG. 5. The  $y$ -phase velocity of the first eigenmode (dash-dotted) and the  $y$ -group velocities of the first (solid) and second (dashed) eigenmode. of the anisotropic lattice for fixed value of  $k_x = \pi/2$ . The phase and group velocities have opposite signs for a range of momenta between  $k_y \cong \pi/2$  and  $2\pi/3$ . This is a characteristic of negative refractive index.

TABLE I. Parameters used in the wave packet dynamics calculation.

Grid	Wave packet	Chebyshev
$N=2100$	$\mathbf{k} = \left(\frac{\pi}{2}, -\frac{\pi}{3}\right)$	$N_{\text{Cheby}}=670$
$a_x=1.0$	$\mathbf{r}_0=(12, 21)$	$\Delta E=50$
$a_y=1.5$	$\sigma=5.0$	
$\Delta y = \frac{a_y}{2} = 0.75$		

$$\psi_{y,z}(\mathbf{r};0) = 0,$$

was evolved similarly to Ref. 1, except that instead of diagonalizing the Hamiltonian, a Chebyshev propagation scheme was utilized.<sup>15</sup> The values of the various simulation parameters are given in Table I.

On this anisotropic lattice and for this particular choice of chosen momentum  $\mathbf{k}=(\pi/2, -(\pi/3))$ , the  $xy$  eigenmodes are not pure. For example, as shown in Fig. 4, at this particular momentum, the lowest energy eigenmode is an exactly half-half mixture of  $x$  and  $y$  polarizations ( $\phi=45^\circ$ ,  $\theta=90^\circ$ ) and thus, this initial state is not an eigenstate of the system.

Figure 6 shows four snapshots of the dynamics of this LSPP Gaussian wave packet, with an additive color scale representing wave function intensity. Blue represents  $x$  polarization LSPP wavefunction intensity, red represents  $y$  polarization, and shades of purple a relative mixture. The initial north-east traveling pure  $x$  polarization (blue) wave packet is, upon hitting the step perturbation, split into a refracted north-east continuing pure  $x$  wave packet (blue) and a reflected north-west heading  $x$  wave packet, both of negligible intensity, and an intense south-east traveling pure  $y$  polarized wave packet (red). This splitting of an incident north-east traveling ray into a south-east traveling one is not observed in conventional optical materials, but is characteristic of

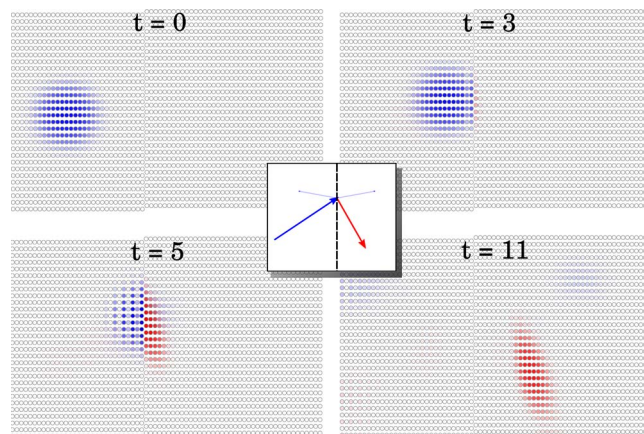


FIG. 6. (Color online) LSPP dynamics on an anisotropic lattice with a perturbation. The color scale is additive, where blue represents  $x$  polarization wave function intensity, red represents  $y$  polarization, and the various shades of purple represent mixed states. The initial north-east traveling pure  $x$  wave function is, upon hitting the perturbation, converted largely into a south-east traveling  $y$  polarized wave function, along with negligible  $x$  polarized reflected and refracted parts. The inset shows a schematic of the corresponding ray diagram. This conversion from a north-east traveling ray to south-east traveling one is analogous to the negative refraction.

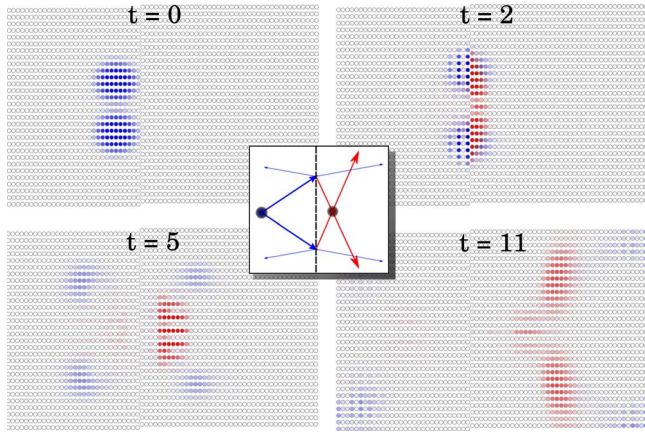


FIG. 7. (Color online) A rudimentary superlens based on the device in Fig. 6. The negative refraction of the two incident  $x$  polarized LSP wave packets into  $y$  polarized ones results in a focusing of the electromagnetic energy on the length scale of a few spacings. The inset shows a simplified ray diagram for the device.

metamaterials such as this. The negative refraction behavior exhibited by this system is a direct result of rich coupling between orthogonal surface plasmon modes and the resulting dispersive properties. This is of particular physical importance, and the design of any potential LSP-based plasmonic device hinges on understanding both the energy-momentum and polarization-momentum dispersion properties.

As a concrete example of the utility of such a device, we now demonstrate how this metamaterial waveguide can use negative refraction to act as a rudimentary superlens.<sup>8</sup> Since the surface plasmon resonance frequency of the nanoparticles can be tuned by choosing the particle size<sup>16</sup> and composition (e.g., a core-shell structure<sup>12,17</sup>), such a device could potentially operate at a wide range of optical frequencies.

Figure 7 shows such a device, where we have reproduced the device simulated in Fig. 6, only with two initial wave packets with opposite  $y$  group velocity, created by tak-

ing their initial momenta to be  $\mathbf{k}_1 = (\pi/2, -(\pi/3))$  and  $\mathbf{k}_2 = (\pi/2, \pi/3)$ , respectively. These two wave packets play the role of rays diverging from a point object somewhere to the left of their starting points (shown as a blue dot in the inset of Fig. 7). As before, the two wave packets are negatively refracted into two  $y$  polarized wave packets, which then cross at a point on the other side of the perturbation. In effect, this device takes diverging  $x$  polarized light and focuses it into  $y$  polarized light a point. What makes this lens so interesting is that it functions on length scales much smaller than the wavelength of light being guided, allowing one to beat the diffraction limit. For example, one could build a device which uses visible light (wavelength on the order of hundreds of nanometers) to resolve features on the order of tens of nanometers. Using such a superlens as a means of subwavelength imaging has enormous potential in a variety of fields, ranging from lithography to biological imaging.

#### IV. RELATION TO ELECTRODYNAMICS

The discussion so far has been in terms of excitations, in a simple excitonic picture of the motion. Here, we relate this discussion to a more usual electrodynamical approach. The connection shows clearly where the approximations are in the discussed approach, and what next steps are needed for a more rigorous theory.

We treat the nanodots as a collection of dipoles. The discussion will be done for one dipole, and then applied to the multiple dot case. The final results do not depend on the explicit form considered for each dipole (at least in the limiting case we consider, where the dipole excitation of each dot is not large). Therefore, for simplicity, we consider a nanodot dipole as one made from a fixed positive charge  $q$  at a position  $\mathbf{x}_0$ , and a negative charge  $q$  at a position  $\mathbf{x}_0 + \mathbf{s}(t)$ , so the dipole is  $\boldsymbol{\mu} = q\mathbf{s}(t)$ .

In the Lorenz gauge, the potential at a point  $\mathbf{x}$  due to a dipole at a position  $\mathbf{x}_0$  is

$$\begin{aligned}
 \Phi(\mathbf{x}, t) &= \int \frac{\delta(t' - t + |\mathbf{x} - \mathbf{x}'|/c)}{|\mathbf{x} - \mathbf{x}'|} [-q[\delta(\mathbf{x}' - \mathbf{x}_0 - \mathbf{s}(t')) - \delta(\mathbf{x}' - \mathbf{x}_0)]] dt' d\mathbf{x}' \\
 &= -q \int \left[ \frac{\delta(t' - t + |\mathbf{x} - \mathbf{x}_0 - \mathbf{s}|/c)}{|\mathbf{x} - \mathbf{x}_0 - \mathbf{s}|} - \frac{\delta(t' - t + |\mathbf{x} - \mathbf{x}_0|/c)}{|\mathbf{x} - \mathbf{x}_0|} \right] dt' \\
 &= -q \left[ \frac{1}{|\mathbf{x} - \mathbf{x}_0 - \mathbf{s}(t - |\mathbf{x} - \mathbf{x}_0 - \mathbf{s}|/c)|} - \frac{1}{|\mathbf{x} - \mathbf{x}_0|} \right] \\
 &= - \left[ \nabla \frac{1}{|\mathbf{x} - \mathbf{x}_0|} \cdot \boldsymbol{\mu} \left( t - \frac{|\mathbf{x} - \mathbf{x}_0 - \mathbf{s}|}{c} \right) \right] \\
 &\cong - \nabla \frac{1}{|\mathbf{x} - \mathbf{x}_0|} \cdot \left( \boldsymbol{\mu} \left( t - \frac{|\mathbf{x} - \mathbf{x}_0|}{c} \right) - \frac{\dot{\boldsymbol{\mu}}}{c} (\nabla |\mathbf{x} - \mathbf{x}_0| \cdot \mathbf{s}) \right). \tag{16}
 \end{aligned}$$

Similarly, the vector potential reads

$$A(\mathbf{x}, t) = \frac{1}{c|\mathbf{x} - \mathbf{x}_0|} \frac{d\mu}{dt} \left( t - \frac{|\mathbf{x} - \mathbf{x}_0|}{c} \right),$$

so that the total electric field is

$$\begin{aligned} \mathbf{E} &= \frac{1}{c} \frac{\partial \mathbf{A}}{\partial t} - \nabla \Phi + \mathbf{E}_{\text{ext}} \\ &= -\frac{1}{c^2 |\mathbf{x} - \mathbf{x}_0|} \frac{d^2 \mu}{dt^2} \left( t - \frac{|\mathbf{x} - \mathbf{x}_0|}{c} \right) \\ &\quad - \frac{\nabla |\mathbf{x} - \mathbf{x}_0|}{c^2} \left( \frac{d\mu}{dt} \left( t - \frac{|\mathbf{x} - \mathbf{x}_0|}{c} \right) \cdot \nabla \frac{1}{|\mathbf{x} - \mathbf{x}_0|} \right) \\ &\quad + \mu \left( t - \frac{|\mathbf{x} - \mathbf{x}_0|}{c} \right) \cdot \nabla \nabla \frac{1}{|\mathbf{x} - \mathbf{x}_0|} + \mathbf{E}_{\text{ext}}, \end{aligned} \quad (17)$$

where we introduced an external field. The first, near-field approximation is to set  $c = \infty$  so that only the  $c$  independent terms survive;

$$\mathbf{E}(\mathbf{x}, t) = \mu_{\mathbf{x}_0}(t) \cdot \nabla \nabla \frac{1}{|\mathbf{x} - \mathbf{x}_0|} + \mathbf{E}_{\text{ext}}. \quad (18)$$

Put differently, the near-field approximation leads back to electrostatics. The near-field approximation is easy to extend but will be valid for short distances.

The next ingredient is the relation between the electric field and the dipole on each dot. If the dots are very closely packed, the electric field on each dot will be strongly space dependent and can reach extremely high values near the surface of the dot, as what happen in surface-enhanced Raman spectroscopy.<sup>18</sup> However, if the packing is not maximal, we can connect the dipole moment with the electric field as

$$\mu(\mathbf{x}, t) = \int_{-\infty}^t \gamma(t - t') \mathbf{E}(\mathbf{x}, t') dt', \quad (19)$$

where we introduced the time-dependent polarizability  $\gamma(t)$ , which can be a tensor in the general case; in frequency space this is, of course,

$$\mu(\mathbf{x}, \omega) = \gamma(\omega) \mathbf{E}(\mathbf{x}, \omega). \quad (20)$$

We can rewrite the equation above as

$$\begin{aligned} \frac{d\mu}{dt}(\mathbf{x}, t) &= \gamma_0 \mathbf{E}(\mathbf{x}, t) + \int \eta(t - t') \mathbf{E}(\mathbf{x}, t') dt', \\ \eta(t) &\equiv \frac{d\gamma}{dt}, \end{aligned} \quad (21)$$

$$\gamma_0 \equiv \gamma(t - t' = 0).$$

The approximation we pursued in the article, of no dissipation, is equivalent to assuming that the time derivative of instantaneous dipole moment only depends on the instantaneous field; this is the same as saying that the polarizability is independent of frequency.

Extending now the discussion to the case of many dipoles, each labeled by an index  $j$ , we get the final equations

$$\frac{d\mu_j}{dt} = \gamma_0 \sum_{k \neq j} \mu_k(t) \cdot \nabla \nabla \frac{1}{|\mathbf{x}_j - \mathbf{x}_k|} + \gamma_0 \mathbf{E}_{\text{ext}}(\mathbf{x}_j, t). \quad (22)$$

This form is completely equivalent to the Schrödinger-type Hamiltonian, if we first identify  $\gamma_0$  with the square of the dipole coupling moment, and also assume that the external electric field is only used to create an instantaneous excitation, after which its effect is removed. We thus find that the “wave function” is simply the polarization at site  $i$ . Two future methodological issues are mentioned below in the appendix; these will be applied in future papers.

Finally, the electrodynamic picture confirms the simple interpretation of the polarization eigenvectors in Eq. (11). The  $F$  tensor ( $3 \times 3$ ) is a near-field equivalent of the permittivity (when the constant diagonal part is removed) so that its eigenvectors are the near-field eigenpolarizations, i.e., those directions of the external field which induce a dipole current that will be parallel to the external field.

The extension of the relation between the dipoles and the electric fields is qualitative, as it is within the electrostatic approximation. The frequency dependence of the relation between the electric field and the dipole moment is due to currents and damping terms, which arise from forces within the dipoles. Therefore, a more quantitative analysis will be needed to account for Lorenz-force contributions and current effects on the equation of motion; nevertheless, the relation between the eigenvectors and the permittivity is qualitatively revealing.

## V. CONCLUSIONS

We presented here a dispersion theory for idealized (weak-field, weak-damping) localized surface plasmon-polariton propagation on evenly spaced lattices of metal nanoparticles. The theory is simple and easy to implement, yet predicts both the energy and polarization character of the eigenmodes of the lattice. We have also connected the theory to electrodynamic simulations.

The interplay between orthogonal modes results in rich physical behavior that, under the appropriate conditions, manifests itself as negative refraction. An understanding of the energy and polarization properties enables one to design devices which support LSPP wave packets that, for certain momenta around the intersections of the adiabatic energy surfaces, readily scatter between different polarization modes. This facile scattering results in quick changes in wave packet direction upon hitting a perturbation. We have demonstrated using time-resolved wave packet simulations that, at least in the low-damping and low-excitation limits, such systems are expected to exhibit negative refractive index. This can be used to construct a crude superlens capable of focusing energy at length scales much less than the wavelength of light being guided.

## ACKNOWLEDGMENTS

This research was supported by the NSF and PRF.

## APPENDIX A: THE SOURCE TERM IN THE TIME-DEPENDENT TREATMENT

In this appendix, we give an outline of an efficient method for propagating an equation such as Eq. (22).

Consider the Schrödinger equation with a source:

$$i\dot{\psi}(t) = H\psi(t) + \sigma(t), \quad (\text{A1})$$

$$\psi(0) = \psi_0.$$

Here,  $\sigma$  is the source function and we assume that  $H$  is time independent. The solution to the problem can be found by noting that  $ie^{-iHt}\partial_t(e^{iHt}\psi) = i\dot{\psi} - H\psi$ . Thus, when  $\sigma$  is a time independent function, the exact solution is

$$\psi(t) = \frac{e^{-iHt} - 1}{H}\sigma + e^{-iHt}\psi_0. \quad (\text{A2})$$

The application of this  $(e^{-iHt} - 1)/H$  can be done easily using Chebyshev polynomials.<sup>15</sup>

Now, for the more general case, when  $\sigma$  is time dependent, we usually consider a pulse of some sort, which dies out over time. If we take, for example,  $\sigma = \sum_n t^{m_n} e^{-\beta_n t} \sigma_n$ , then this is also tractable:

$$\psi = -i \sum_n I_n(\hat{H}) \sigma_n + e^{iHt} \psi_0, \quad (\text{A3})$$

where

$$I_n(\alpha) = e^{-\alpha t} \int_0^t t'^{m_n} e^{(\alpha - \beta_n)t'} dt'. \quad (\text{A4})$$

Once again  $I_n(H)\sigma_n$  can be easily applied using efficient and fast Chebyshev propagation.<sup>15</sup> The only caveat is that if one needs a large expansion, this might be expensive.

## APPENDIX B: PROPAGATION WITH DISSIPATION

To account for dissipation, we need to solve equations of the form

$$i\dot{\psi}(t) = H\psi(t) + \int_0^t \gamma(t-t')\psi(t')dt', \quad (\text{B1})$$

assuming that we can approximate

$$\gamma(\tau) = \sum_{n=1}^N a_n e^{-\eta_n \tau}. \quad (\text{B2})$$

We can convert the equation to an instantaneous set of  $N+1$  equations.<sup>19</sup> Indeed, using

$$i\partial_t(e^{iHt}\psi(t)) \equiv i\partial_t(\phi(t)) = \sum_{n=1}^N a_n \psi_n(t),$$

where

$$\psi_n(t) = e^{iHt} \int_0^t e^{-\eta_n(t-t')} \psi(t') dt' = \int_0^t e^{(iH - \eta_n)(t-t')} \phi(t') dt'.$$

Taking the time derivative of this last equation, we obtain a set of coupled instantaneous equations:

$$\dot{\psi}_n(t) = \phi(t) + (iH - \eta_n)\psi_n, \quad (\text{B3})$$

$$i\dot{\phi}(t) = \sum_{n=1}^N a_n \psi_n(t).$$

Thanks to the removal of memory, a source term can now be combined with this approach, as was done in Appendix A.

- <sup>1</sup>R. Baer, K. Lopata, and D. Neuhauser, J. Chem. Phys. **126**, 014705 (2007).
- <sup>2</sup>S. A. Maier, P. G. Kik, and H. A. Atwater, Phys. Rev. B **67**, 205402 (2003); F. I. Baida, D. Van Labeke, Y. Pagani, B. Guizal, and M. Al Naboulsi, J. Microsc. **213**, 144 (2004).
- <sup>3</sup>W. H. Weber and G. W. Ford, Phys. Rev. B **70**, 125429 (2004).
- <sup>4</sup>M. Quinten, A. Leitner, J. R. Krenn, and F. R. Aussenegg, Opt. Lett. **23**, 1331 (1998); R. Quidant, C. Girard, J. C. Weeber, and A. Dereux, Phys. Rev. B **69**, 085407 (2004).
- <sup>5</sup>S. A. Maier, P. G. Kik, H. A. Atwater, S. Meltzer, E. Harel, B. E. Koel, and A. A. G. Requicha, Nat. Mater. **2**, 229 (2003).
- <sup>6</sup>L. A. Sweatlock, S. A. Maier, H. A. Atwater, J. J. Penninkhof, and A. Polman, Phys. Rev. B **71**, 235408 (2005); J. R. Krenn, J. C. Weeber, A. Dereux, E. Bourillot, J. P. Goudonnet, B. Schider, A. Leitner, F. R. Aussenegg, and C. Girard, *ibid.* **60**, 5029 (1999).
- <sup>7</sup>G. Veselago and E. E. Narimanov, Nat. Mater. **5**, 759 (2006); V. G. Veselago, Sov. Phys. Usp. **10**, 509 (1968).
- <sup>8</sup>J. B. Pendry, Phys. Rev. Lett. **85**, 3966 (2000).
- <sup>9</sup>N. Fang, H. Lee, C. Sun, and X. Zhang, Science **308**, 534 (2005).
- <sup>10</sup>S. K. Gray and T. Kupka, Phys. Rev. B **68**, 045415 (2003).
- <sup>11</sup>K. L. Kelly, A. A. Lazarides, and G. C. Schatz, Comput. Sci. Eng. **3**, 67 (2001); A. A. Lazarides and G. C. Schatz, J. Phys. Chem. B **104**, 460 (2000).
- <sup>12</sup>R. Baer, D. Neuhauser, and S. Weiss, Nano Lett. **4**, 85 (2004).
- <sup>13</sup>E. Prodan and P. Nordlander, J. Chem. Phys. **120**, 5444 (2004).
- <sup>14</sup>A. Melikyan and H. Minassian, Appl. Phys. B: Lasers Opt. **78**, 453 (2004).
- <sup>15</sup>R. Kosloff, J. Phys. Chem. **92**, 2087 (1988).
- <sup>16</sup>U. Kreibig and M. Vollmer, *Optical Properties of Metal Clusters* (Springer-Verlag, Berlin, 1994); S. Link and M. A. El-Sayed, J. Phys. Chem. B **103**, 4212 (1999).
- <sup>17</sup>E. Prodan and P. Nordlander, Nano Lett. **3**, 543 (2003).
- <sup>18</sup>A. Nitzan and L. E. Brus, J. Chem. Phys. **75**, 2205 (1981).
- <sup>19</sup>C. Meier and D. J. Tannor, J. Chem. Phys. **111**, 3365 (1999).